Journal of
MATERIALS RESEARCH

System Bi–Sr–O: Synergistic measurements of thermodynamic properties using oxide and fluoride solid electrolytes

K. T. Jacob[a] and K. P. Jayadevan
Materials Research Centre and Department of Metallurgy, Indian Institute of Science, Bangalore 560 012, India

(Received 5 May 1997; accepted 10 November 1997)

Phase equilibrium and electrochemical studies of the ternary system Bi–Sr–O indicate the presence of six ternary oxides (Bi_2SrO_4, $Bi_2Sr_2O_5$, $Bi_2Sr_3O_6$, $Bi_4Sr_6O_{15}$, $Bi_{14}Sr_{24}O_{52}$, and $Bi_2Sr_6O_{11}$) and three solid solutions (δ, β, and γ). An isothermal section of the phase diagram is established at 1050 K by phase analysis of quenched samples. Three compounds, $Bi_4Sr_6O_{15}$, $Bi_{14}Sr_{24}O_{52}$, and $Bi_2Sr_6O_{11}$, contain Bi^{5+} ions. The stability of these phases is a function of oxygen partial pressure. The chemical potentials of SrO in two-phase fields are determined as a function of temperature using solid-state cells based on single crystal SrF_2 as the electrolyte. Measurement of the emf of cells based on SrF_2 as a function of oxygen partial pressure in the gas at constant temperature gives information on oxygen content of the compounds present at the electrodes. The chemical potentials of Bi_2O_3 in two-phase fields of the pseudobinary Bi_2O_3–SrO are measured using cells incorporating $(Y_2O_3)ZrO_2$ as the solid electrolyte. The standard free energies of formation of the ternary oxides are calculated independently using emfs of different cells. The independent assessments agree closely; the maximum difference in the value of ΔG_f° $(Bi_{2m}Sr_nO_p)/(m + n)$ is $\pm$ 350 J/mol of component binary oxides. The results are discussed in the light of the phase diagram and compared with calorimetric and chemical potential measurements reported in the literature. The combined use of emf data from cells incorporating fluoride and oxide electrolytes enhances the reliability of derived data.

I. INTRODUCTION

As a part of the systematic studies on phase equilibria and thermodynamic properties of the quaternary system Bi–Ca–Sr–Cu–O which contains several superconducting oxides, measurements have been made on the ternary system Bi–Sr–O. Phase diagrams provide indispensable guidelines for the control of impurity phases in the preparation of high T_c oxides. Thermodynamic data on subsystems are fundamental inputs for computation of phase equilibria in a multicomponent oxide system as a function of temperature and partial pressure of oxygen. Because of their high oxygen-ion conductivity, Bi_2O_3-based solid solutions are also of interest as electrolytes for solid oxide fuel cells.

The phase diagram for the system Bi_2O_3–SrO has been investigated by a number of researchers. Guillermo *et al.*[1] and Conflant *et al.*[2] used high temperature x-ray diffraction (HTXRD) and differential thermal analysis (DTA) to establish phase relations in the pseudobinary system in air. The diagrams proposed are very similar and are probably based to a large extent on a common database. Conflant *et al.*[2] have slightly altered the phase transition temperature of β-phase. Hence, only the most recent paper[2] will be referred to in further discussions. Levin and Roth[3] used HTXRD to study Bi_2O_3-rich solid solutions. XRD on quenched samples was employed by Roth *et al.*,[4] Hwang *et al.*,[5] and Vstavskaya *et al.*[6] to map the phase diagram in air. Phase diagrams of Roth *et al.*[4] and Hwang *et al.*[5] also appear to be based on the same experimental information. DTA/TGA (thermogravimetric analysis) and XRD were employed by Abbattist *et al.*[7] to study phase relations for SrO-rich compositions in pure O_2, air, and silica ampules sealed under vacuum. Jacob and Mathews[8] have investigated the ternary system $BiO_{1.5}$–SrO–CuO at 1123 K in pure O_2 at ambient pressure. Slobodin *et al.*[9] have investigated the ternary system in the region $Bi_2O_3/SrO > 0.5$ in air at 1023 K. Strictly, this diagram is a projection of phase relations in the ternary Bi_2O_3–SrO–O ($P_{O_2} = 2.12 \times 10^4$ Pa) from the oxygen apex onto the Bi_2O_3–SrO isopleath. The diagram shows that the phases that will appear if compositions along the Bi_2O_3–SrO pseudobinary are equilibrated in air. Phase relations in the binary Bi_2O_3–SrO under the specified conditions can be obtained from these studies on the ternary system. A review of the reported ternary compounds indicates that several of these contain excess oxygen and do not lie on the Bi_2O_3–SrO join of the ternary system Bi–Sr–O. Although there are

[a]Address correspondence to this author.

some common features in the results obtained by various investigators, there are differences in the stability ranges of many phases. Among the important differences are the extended stability of β-phase and reduced stability of Bi_2SrO_4 in the phase diagram of Conflant *et al.*[2] compared to that of Hwang *et al.*[5] Normally, HTXRD used by the first group of researchers[2] is more reliable for mapping high temperature phase relations than room temperature XRD of quenched samples employed by the second group.[5] However, because of the volatility of Bi_2O_3, the sample composition can change during prolonged high temperature exposure unless special containment techniques are employed.[8] More recent work by Vstavskaya *et al.*[6] is in better agreement with the phase diagram proposed by Hwang *et al.*[5] An evaluated "phase diagram" for the system Bi_2O_3–SrO in air is displayed in Fig. 1 to provide a focus for discussion. Strictly, this diagram is a projection of phase relations in the ternary Bi_2O_3–SrO–O ($P_{O_2} = 2.12 \times 10^4$ Pa) from the oxygen apex onto the Bi_2O_3–SrO isopleath. The diagram shows the phases that will appear if compositions along the Bi_2O_3–SrO pseudobinary are equilibrated in air. Phase relations for $X_{SrO} > 0.67$ are primarily based on the results of this study. Crystallographic information on the compounds is summarized in Table I.

The solubility of SrO in low temperature α–Bi_2O_3 appears to be negligible.[2] Hwang *et al.*[5] indicate a small solubility of SrO in α–Bi_2O_3, without experimental evidence. There is considerable solubility of SrO in δ–Bi_2O_3,[1–5] but the solid solution range is less extensive than for the corresponding Bi_2O_3–CaO system.[10] The β-phase with a rhombohedral unit cell extends from $X_{SrO} \approx 0.2$ to $X_{SrO} \approx 0.42$ at 1000 K[5,6] and melts congruently at 1225 K.[5,6] The β-phase exists in two forms; the high temperature form β_1 is stable above 906 to 987 K, depending on composition.[2] The high temperature phase exhibits high oxygen ion conductivity,[11] but cannot be retained at room temperature by quenching.

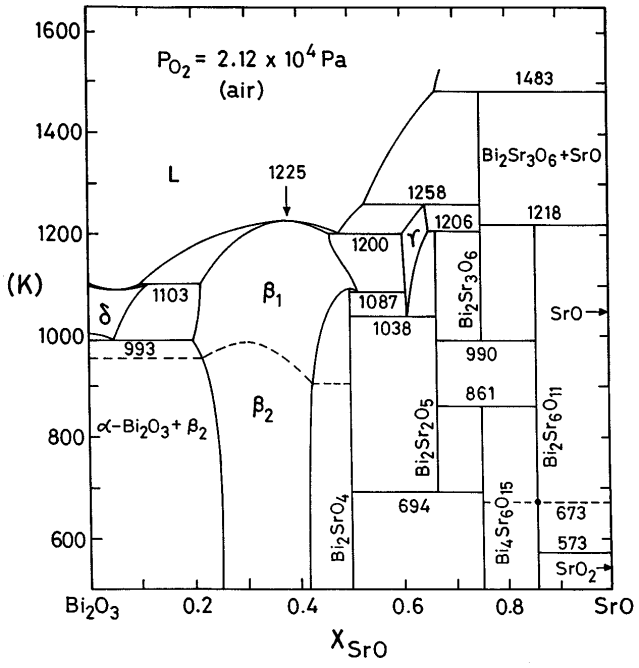

FIG. 1. Projection of phase relations in the system Bi_2O_3–SrO–O in air onto the Bi_2O_3–SrO isopleath.

Conflant *et al.*[2] found that the compound Bi_2SrO_4 decomposes to β_1 and γ at 1053 K using HTXRD. According to Hwang *et al.*,[5] the compound Bi_2SrO_4 undergoes a phase transition to a high temperature form with slightly lower SrO content at 1098 K. The high temperature form decomposes to liquid and γ-phase at 1213 K. Zinkevich *et al.*[12] report melting of stoichiometric Bi_2SrO_4 at 1214 K. Jacob and Mathews[8] identified the compound in samples quenched from 1123 K. Vstavskaya *et al.*[6] show the decomposition of Bi_2SrO_4 to β and $Bi_2Sr_2O_5$ at 1188 K. Emf results obtained in this study suggest congruent transformation of Bi_2SrO_4 to β_1 solid solution. The rhombohedral solid solution (β_1) cannot be quenched to room temperature without crystallization of Bi_2SrO_4. At higher temperatures the compound composition enters the two-phase field $\beta + \gamma$. If Bi_2SrO_4 decomposed to β_1 and γ as proposed by Conflant *et al.*,[2] it should have been possible to retain the high temperature two-phase structure by quenching. Figure 1 is based on the findings of Conflant *et al.*[2] and results of this study, both of which are based on high-temperature measurements.

There is general agreement on the stability range of the γ-phase and the upper stability limit of $Bi_2Sr_2O_5$.[2,5] The compound $Bi_2Sr_2O_5$ decomposes to γ and $Bi_2Sr_3O_6$ at 1206 K. The unit cell of $Bi_2Sr_2O_5$ has orthorhombic symmetry, but there is variability in the reported space group.[1,4,21] Torardi *et al.*[21] found evidence for the existence of a superlattice along the *c*-direction in long exposure precession photographs of single crystals. They attributed the superlattice to the ordering of oxygen vacancies and the resultant replacement of Bi atoms. Conflant *et al.*[2] suggest decomposition of the compound $Bi_2Sr_2O_5$ to Bi_2SrO_4 and SrO at 913 K. This is not supported by the studies of Abbattista *et al.*[7] who show the presence of two other stable phases $Bi_4Sr_6O_{15}$ and $Bi_2Sr_6O_{11}$ between $Bi_2Sr_2O_5$ and pure SrO. The phase relations shown in Fig. 1 for $X_{SrO} > 0.67$ are based on the results obtained in this study; supported by the findings of Abbattista *et al.*[7]

The compound $Bi_2Sr_3O_6$ decomposes to liquid and SrO at 1483 K.[5] There is controversy on the low temperature stability limit of $Bi_2Sr_3O_6$. Conflant *et al.*[2] indicate the compound is stable only above 1083 K, whereas Hwang *et al.*[5] show the compound to be stable down to 973 K. Abbattista *et al.*[7] show the low temperature stability limit as 873 K in pure O_2, but the decomposition

TABLE I. Crystallographic data on compounds in the system Bi–Sr–O.

Compound	Lattice parameters						Structure	Ref.
	a (nm)	b (nm)	c (nm)	α	β	γ		
$\alpha-Bi_2O_3$	0.5849	0.8165	0.7510		112.98°		Monoclinic, $P2_{1/C}$	14
$\delta-Bi_2O_3$ (T = 1047 K)	0.5660						Cubic, $Fm3m$	14
SrO	0.5160						Cubic, $Fm3m$	15
SrO_2	0.3563		0.6616				Tetragonal, $I4/mmm$	16
$BiSr_2$	0.5012		1.7683				Tetragonal, $I4/mmm$	
β–solid solution (X_{SrO} = 0.4)								
β_2								
T = 300 K	0.3970		2.8540			120°	Rhombohedral, $R\bar{3}m$	18
T = 600 K	0.3983		2.8690			120°	Rhombohedral, $R\bar{3}m$	18
β_1								
T = 1050 K	0.4011		2.9011			120°	Rhombohedral, $R\bar{3}m$	18
β_2, X_{SrO}								
0.25	0.3976		2.8102				Rhombohedral, $R\bar{3}m$	19
0.33	0.3967		2.8300					19
0.40	0.3968		2.8481					19
Bi_2SrO_4	1.9300	0.4358	0.6106		94.80°		Monoclinic, $C2/m$	20
γ solid solution	1.3239		0.4257				Tetragonal, $I4/m$	1
$Bi_2Sr_2O_5$	1.4261	0.6160	0.7642				Orthorhombic, $Pnma$	21
	1.4293	0.6172	0.7651				Orthorhombic, $Pcmm$	1, 22
	1.4307	0.6171	0.3826				Orthorhombic, $Cmcm$	4, 23
$Bi_2Sr_3O_6$	1.2526		1.8331			120°	Rhombohedral, $R\bar{3}m$	4
$Bi_4Sr_6O_{15}$	1.7236	1.7102	1.1875				Orthorhombic	7
$Bi_2Sr_6O_{11}$	1.6933		1.6648				Tetragonal	7
	0.6009		0.8372				Tetragonal, $I4/m$	24, 25
	0.6009		5.8663			120°	Rhombohedral	4
	1.7147	1.6758	1.6998				Orthorhombic	6, 26

involves a four-phase equilibrium.[7] Abbattista *et al.*[7] also suggest the presence of an oxygen-rich compound with the same Bi/Sr ratio ($Bi_4Sr_6O_{15}$) which is stable below ~973 K. The formation of this oxygen-rich compound also involves a four-phase equilibrium. The occurrence of two four-phase equilibria in such close proximity is rather unlikely. Hwang *et al.*[5] have identified a new compound $Bi_2Sr_6O_9$ which was not detected by Conflant *et al.*[2] The compound has also been identified by Jacob and Mathews[8] at 1123 K. More recent studies, however, show that this compound has excess oxygen and can be represented as $Bi_2Sr_6O_{11}$.[7,13] The Bi/Sr ratio is identical for both designations. The excess oxygen was detected using TGA and DTA. The compound $Bi_2Sr_6O_{11}$ was found to decompose to $Bi_2Sr_3O_6$, SrO, and O_2 between 1293 K and 1363 K.[7,13] There is a phase transition associated with this compound at 673 K.[2] The low temperature form appears to have tetragonal symmetry,[7,24,25] although reported cell parameters show discrepancies. The high-temperature form of $Bi_2Sr_6O_{11}$ can be quenched to room temperature. At moderate cooling rates both the high and low temperature forms may be present in the sample, making the determination of the correct crystal structure more difficult.

Baek and Virkar[27] have used galvanic cells with SrF_2 solid electrolyte to determine the activity-composition relationship in the system Bi_2O_3–SrO in the temperature range 850–975 K. Surprisingly, measurements on electrodes with average compositions in the range $0.59 < K_{SrO} < 0.8$ gave approximately the same emf. According to Fig. 1, these compositions should fall in at least two separate phase fields. The emf data of Baek and Virkar[27] are not sufficient to derive free energies of formation of interoxide compounds. Idemoto *et al.*[28] have measured the enthalpies of formation of six compositions which correspond to compounds Bi_2SrO_4, $Bi_2Sr_2O_5$, $Bi_2Sr_3O_6$, $Bi_2Sr_6O_{11}$, and solid solutions β and γ. The Bi ion was found to be in the trivalent state by titration in all the samples. This conflicts with other information which indicates that Bi is in the pentavalent state in the compound $Bi_2Sr_6O_{11}$.[7,13,29] A reinvestigation of the ternary system Bi–Sr–O, with emphasis on the thermodynamic properties, would be useful to resolve the discrepancies reported in the literature. Phase equilibria under different conditions can be readily computed from the thermodynamic data.

Measurement strategy: Combined use of oxide and fluoride electrolytes

The activity of SrO in various phase fields of the system Bi–Sr–O can be measured as a function of temperature using solid-state cells based on SrF_2 under controlled partial pressure of oxygen. The electrolyte

SrF_2 is a fluoride ion conductor with transport number $t_F - 0.99$. The emf of a cell based on SrF_2 is directly related to the difference in the chemical potential of F_2 at the two electrodes. The chemical potential of fluorine is established at each electrode by the exchange reaction,

$$SrF_2 + \frac{1}{2} O_2 \longrightarrow SrO + F_2 , \qquad (1)$$

where SrO is present at unit activity at the reference electrode and at reduced activity at the working electrode. To obtain free energies of formation of interoxide compounds from the emf data, Gibbs–Duhem integration across the single-phase field of β is necessary. Accurate measurement of the chemical potential of SrO in single-phase field is rather difficult, since the working electrode in such a case is monovariant. Small perturbations during measurement can cause changes in emf. Higher accuracies are obtained when chemical potentials in two-phase fields are measured under controlled oxygen partial pressure, since equilibria defining potentials at the electrodes are then invariant at constant temperature and total pressure.

Information on oxygen nonstoichiometry or oxygen content of ternary oxides can be obtained by measuring the emf of cells based on SrF_2 as a function of oxygen partial pressure at the electrodes at constant temperature.[30,31] This technique is helpful in determining excess oxygen in some ternary oxides present in the system Bi–Sr–O.

In principle, the standard free energy of formation of interoxide compounds can be obtained from measurements of the activity of Bi_2O_3 in various phase fields starting from the SrO side. The accuracy of such measurements decreases as one moves progressively toward compounds richer in Bi_2O_3. For example, to obtain the free energy of formation of Bi_2SrO_4 at 1050 K, emf of four cells involving phase fields SrO + $Bi_2Sr_3O_6$ + Bi, $Bi_2Sr_3O_6$ + $Bi_2Sr_2O_5$ + Bi, $Bi_2Sr_2O_5$ + γ-phase + Bi, and γ-phase + Bi_2SrO_4 + Bi have to be combined with the consequent accumulation of errors.

The inaccuracies introduced by Gibbs–Duhem integration across the β-phase field and combining emf of several cells can be overcome by independent measurements of the activity of both SrO and Bi_2O_3 in two-phase fields using different kinds of solid-state cells. The free energy formation of each ternary oxide lying on the Bi_2O_3–SrO join can then be obtained from activities of SrO and Bi_2O_3 in two-phase fields on either side of the compound under consideration. For the compound $Bi_{2m}Sr_nO_{3m+n}$, the standard Gibbs energy of formation from component oxides is given by:

$$\Delta G^0_{f,0x} = m\Delta\mu_{Bi_2O_3} + n\Delta\mu_{SrO} = RT(m \ln a_{Bi_2O_3} + n \ln a_{SrO}) , \qquad (2)$$

where values for chemical potentials and activities are those in equilibrium with the compound. Two values for the free energy of formation of each compound are obtained when activities of both components are measured in all the two-phase fields of the pseudobinary system Bi_2O_3–SrO, thus providing an independent check on the accuracy of measurements. The standard Gibbs energies of formation of phases that contain excess oxygen and lie above the Bi_2O_3–SrO join are obtained from measurements on cells based on SrF_2, relative to values for $Bi_2Sr_3O_6$ and $Bi_2Sr_2O_5$. Measurements are made on more than the minimum number of cells required to obtain thermodynamic data on compounds and solid solutions, so that the derived information can be cross-checked for internal consistency. For the correct design of galvanic cells, phase relations in the ternary system Bi–Sr–O should be known. Hence, a study of the isothermal section of the phase diagram at 1050 K is undertaken first.

II. EXPERIMENTAL

A. Materials

Starting materials used for the preparation of interoxide compounds in the system Bi_2O_3–SrO were fine powders of Bi_2O_3 and $SrCO_3$, each of 99.99% purity, obtained from Johnson Matthey Chemicals Ltd. Anhydrous $SrCO_3$ contained in a platinum crucible was decomposed under vacuum at 1073 K to SrO. The SrO thus formed was found to be highly reactive. Fine powders of the component oxides were mixed in appropriate stoichiometric ratio, pelletized at ~20 MPa, contained in Pt crucible, and sealed in quartz ampules under reduced pressure of $\sim 2 \times 10^4$ Pa. The ampules were heated at 1073 K for ~50 h and at 1173 K for ~25 h. Formation of interoxide compounds Bi_2SrO_4, $Bi_2Sr_2O_5$, $Bi_2Sr_3O_6$, $Bi_2Sr_6O_{11}$, β-phase ($0.123 < X_{SrO} < 0.423$), and γ-phase ($0.605 < X_{SrO} < 0.635$) was confirmed by x-ray diffraction. The compound $Bi_4Sr_6O_{15}$ was obtained by heating $Bi_2Sr_3O_6$ in pure oxygen at ambient pressure at 920 K for ~6 h. The compound $Bi_{14}Sr_{24}O_{52}$ was obtained from component oxides only when heated in pure oxygen at ~1050 K.

Alloys and intermetallic compounds in the system Bi–Sr were made by melting or reacting together pure metals in closed iron crucibles under flowing Ar gas. The metals were 99.9% pure. High purity Ar gas used was dehydrated by passing through anhydrous $MgClO_4$ and P_2O_5, and deoxidized by passing through Cu turnings at 750 K and Ti granules at 1150 K.

Optical grade single-crystal SrF_2 pellets of 5 mm thickness and 10 mm diameter were obtained from Aldrich Chemicals. Yttria-stabilized zirconia crucibles contained approximately 8 mol % Y_2O_3. High purity O_2 gas (99.999%) was passed over CuO at 800 K to convert

residual CO and H_2 to CO_2 and H_2O, respectively. CO_2 was absorbed by passing the gas through NaOH. The gas was subsequently dried by passage through columns containing silica gel, anhydrous $MgClO_4$, and P_2O_5. Gas mixtures containing Ar and O_2 were prepared by mixing metered streams of the two gases. Mass-flow controllers were used to meter each gas fed into a mixing tower filled with glass beads.

B. Phase relations in the system Bi–Sr–O

Phase relations at 1050 K were explored by equilibrating different mixtures of alloys and compounds for ~100 h, followed by quenching in chilled Hg and phase identification using optical microscopy, XRD, and EDAX. Preliminary experiments indicated that ~60 h was sufficient to attain equilibrium. Further heat treatment did not change the composition of the samples. Samples containing oxides were held in closed stabilized-zirconia crucibles. Each sample pellet was placed on a small presintered sacrificial pellet of the same composition. The zirconia crucibles were sealed in quartz ampules under a reduced pressure of $\sim 2 \times 10^4$ Pa. Samples containing oxide mixtures were also equilibrated under pure oxygen at a pressure of 1.01×10^5 Pa to check for the presence of phases containing excess oxygen. The mass of each sample was determined before and after equilibration. Mixtures containing metallic phase were equilibrated in closed iron containers kept under prepurified inert gas flowing at a rate of ~3 ml/s. Phase composition of quenched samples was determined using XRD, SEM, and EDAX. For accurate determination of composition using EDAX, the electron beam was focused at the center of grains larger than 10 μm. The composition was found to be invariant across large grains. Different grains belonging to the same phase had identical composition. Pure high-density pellets of SrO and Bi_2O_3 were used as standards. To check for the attainment of equilibrium, samples of the same overall composition were prepared using different starting materials. Approach to equilibrium was thus verified from different directions.

C. Emf measurements on cells based on $(Y_2O_3)ZrO_2$ as the solid electrolyte

A schematic diagram of the cell used is shown in Fig. 2. The reference electrode consisting of an equimolar mixture of Bi and Bi_2O_3 powders was contained in a stabilized-zirconia crucible with an Os wire embedded in the mixture. The metal Os was found to be inert to liquid Bi and its oxides. A mixture of Bi and Bi_2O_3 was tightly packed inside the crucible by ramming with a steel rod. The crucible was covered with a stabilized-zirconia lid. The contacting surface of the crucible and the lid were polished using diamond paste. The Os lead

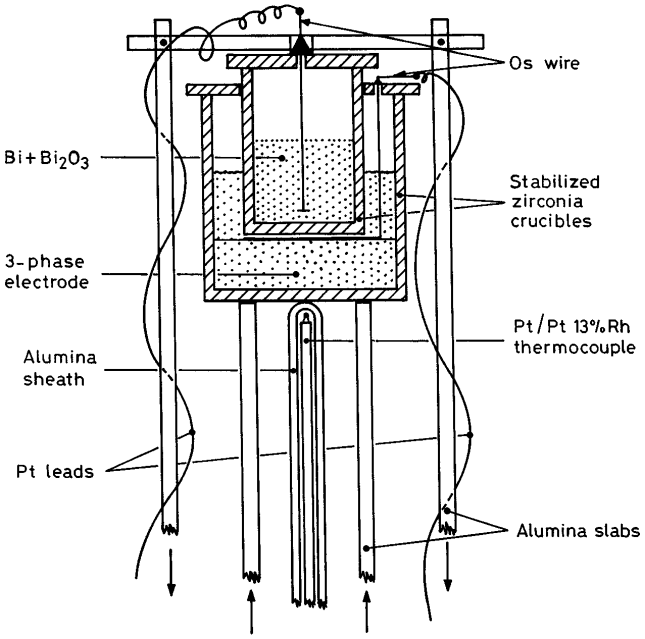

FIG. 2. Schematic diagram of the cell used for emf measurements employing $(Y_2O_3)ZrO_2$ as the solid electrolyte.

was taken out through a small hole in the lid. The aperture was sealed with a zirconia-based cement.

The working three-phase electrode was contained in a larger zirconia crucible. The electrode was prepared by taking Bi and two coexisting oxide phases belonging to the pseudobinary system Bi_2O_3–SrO in the molar ratio 1 : 1.5 : 1.5. The mixture was pelletized at ~20 MPa pressure before placing in the zirconia crucible. Although Bi metal was liquid at the temperatures of measurement, it did not segregate at the bottom of the container. Fine droplets of liquid Bi in the pellet were held by surface tension forces between surrounding oxide grains. The smaller zirconia crucible containing the reference electrode was pressed down against the three-phase electrode pellet by a system of alumina tubes, slabs, and springs. The annular space between the two zirconia crucibles was packed with the three-phase mixture, composition of which was identical to that of the working electrode. The outer solid electrolyte crucible was also closed with a lid containing a circular hole in the center and an aperture for Os wire contacting the working electrode. The Os wires were connected to Pt leads outside each crucible. Since both Os/Pt junctions were at the same temperature, there was no thermoelectric contribution to the cell emf. The cell assembly shown in Fig. 2 was placed inside a vertical alumina tube and suspended in the even-temperature zone (± 1 K) of a resistance furnace. A stainless steel sheet was wrapped around the alumina tube and earthed to minimize induced emf on cell leads. The top and bottom ends of the vertical alumina tube enclosing the cell were closed with brass

caps. The brass caps were provided with a gas inlet and outlet and insulated provision for electric leads. The alumina tube was flushed with pre purified Ar gas at a flow rate of ~3 ml/s. The emf developed between the Pt leads was measured using a high impedance voltmeter. Temperature of the cell was measured by a Pt/Pt-13% Rh thermocouple placed adjacent to the zirconia crucible. The temperature was controlled to ±1 K.

The emf of the following cells were measured as a function of temperature:

$$\text{Pt, Os, SrO} + \text{Bi}_2\text{Sr}_3\text{O}_6 + \text{Bi}|(\text{Y}_2\text{O}_3)\ \text{ZrO}_2|\ \text{Bi} + \text{Bi}_2\text{O}_3,\ \text{Os, Pt}, \quad \text{(I)}$$

$$\text{Pt, Os, Bi}_2\text{Sr}_3\text{O}_6 + \text{Bi}_2\text{Sr}_2\text{O}_5 + \text{Bi}|(\text{Y}_2\text{O}_3)\ \text{ZrO}_2|\ \text{Bi} + \text{Bi}_2\text{O}_3,\ \text{Os, Pt}, \quad \text{(II)}$$

$$\text{Pt, Os, Bi}_2\text{Sr}_2\text{O}_5 + \text{Bi}_2\text{SrO}_4 + \text{Bi}|(\text{Y}_2\text{O}_3)\ \text{ZrO}_2|\ \text{Bi} + \text{Bi}_2\text{O}_3,\ \text{Os, Pt}, \quad \text{(III)}$$

$$\text{Pt, Os, Bi}_2\text{SrO}_4 + \beta\text{-phase} + \text{Bi}|(\text{Y}_2\text{O}_3)\ \text{ZrO}_2|\ \text{Bi} + \text{Bi}_2\text{O}_3,\ \text{Os, Pt}. \quad \text{(IV)}$$

The reversibility of emfs was checked by microcoulometric titration in both directions. Emf was found to return to the same value after each titration. The chemical potentials at the electrodes were altered by essentially an infinitesimal amount during each titration. Since the chemical potentials returned to the same value after very small displacements in opposite directions, attainment of equilibrium was demonstrated. Emfs were independent of the flow rate of Ar gas (2 to 5 ml/s) around the cell and reproducible on temperature cycling. After each emf run electrodes were examined by x-ray diffraction. No significant change in the phase composition of the electrodes was noted.

D. Emf measurements on cells based on SrF_2 as the solid electrolyte

A schematic diagram of the cell assembly incorporating SrF_2 as the electrolyte is shown in Fig. 3. The electrode pellets were spring-loaded on either side of a transparent single crystal of SrF_2, with a thin Pt gauze placed between each electrode and the solid electrolyte. Pt wires, spot-welded to the Pt gauze on either side of the electrolyte, provided electrical leads to a high impedance voltmeter (10^{13} Ω). The pellets were held together under pressure through a system consisting of springs, an alumina rod, and a flat-bottomed alumina tube with a section cut away parallel to its axis as shown in the figure. Direct contact of the electrode pellets with alumina rod or tube was prevented by inserting Pt foils between them. The cell was maintained under dry flowing O_2 at a pressure of 1.01×10^5 Pa.

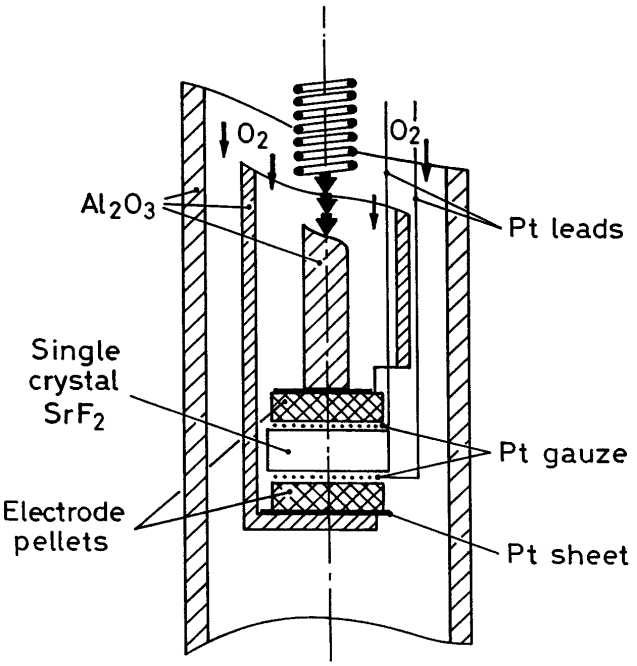

FIG. 3. Schematic diagram of the apparatus used for emf measurements on cells based on single-crystal SrF_2 as the electrolyte.

In preliminary experiments, transparent SrF_2 crystals were found to become translucent during the run. Fine opaque precipitates appeared on the outer surface of SrF_2 crystals. These precipitates were identified by selected area electron diffraction as SrO. They apparently formed by the reaction of the crystal with residual moisture in the gas:

$$\text{SrF}_2(\text{s}) + \text{H}_2\text{O}(\text{g}) \longrightarrow \text{SrO}(\text{s}) + 2\,\text{HF}(\text{g}). \quad \text{(3)}$$

The precipitation of SrO was minimized by degassing the alumina tubes and rods under vacuum and by using an improved drying procedure for O_2 gas. It can be shown from thermodynamic considerations[32] that SrF_2 will not react with dry O_2 to form SrO and F_2 at $\{(P_{F2}/P^0)\} > 10^{-10}$ unless the chemical potential of SrO is very low ($\Delta\mu_{SrO} < -360$ kJ/mol at 1100 K).

The emfs of the following cells were measured as a function of temperature:

$$\text{Pt, O}_2, \text{SrO}|\text{SrF}_2|\text{Bi}_2\text{Sr}_6\text{O}_{11} + \text{Bi}_2\text{Sr}_3\text{O}_6, \text{O}_2, \text{Pt}, \quad \text{(V)}$$

$$\text{Pt, O}_2, \text{SrO}|\text{SrF}_2|\text{Bi}_2\text{Sr}_6\text{O}_{11} + \text{Bi}_{14}\text{Sr}_{24}\text{O}_{52}, \text{O}_2, \text{Pt}, \quad \text{(VI)}$$

$$\text{Pt, O}_2, \text{SrO}|\text{SrF}_2|\text{Bi}_2\text{Sr}_6\text{O}_{11} + \text{Bi}_4\text{Sr}_6\text{O}_{15}, \text{O}_2, \text{Pt}, \quad \text{(VII)}$$

$$\text{Pt, O}_2, \text{SrO}|\text{SrF}_2|\text{Bi}_2\text{Sr}_3\text{O}_6 + \text{Bi}_2\text{Sr}_2\text{O}_5, \text{O}_2, \text{Pt}, \quad \text{(VIII)}$$

$$\text{Pt, } O_2, \text{ SrO}|SrF_2|Bi_{14}Sr_{24}O_{52} + Bi_2Sr_2O_5, O_2, \text{ Pt}, \quad \text{(IX)}$$

$$\text{Pt, } O_2, \text{ SrO}|SrF_2|Bi_4Sr_6O_{15} + Bi_2Sr_2O_5, O_2, \text{ Pt}, \quad \text{(X)}$$

$$\text{Pt, } O_2, \text{ SrO}|SrF_2|Bi_2Sr_2O_5 + \gamma\text{-phase}, O_2, \text{ Pt}, \quad \text{(XI)}$$

$$\text{Pt, } O_2, \text{ SrO}|SrF_2|Bi_2Sr_2O_5 + Bi_2SrO_4, O_2, \text{ Pt}, \quad \text{(XII)}$$

$$\text{Pt, } O_2, \text{ SrO}|SrF_2|\gamma\text{-phase} + Bi_2SrO_4, O_2, \text{ Pt}, \quad \text{(XIII)}$$

$$\text{Pt, } O_2, \text{ SrO}|SrF_2|Bi_2SrO_4 + \beta\text{-phase}, O_2, \text{ Pt}, \quad \text{(XIV)}$$

$$\text{Pt, } O_2, \text{ SrO}|SrF_2|\beta\text{-phase} + \gamma\text{-phase}, O_2, \text{ Pt}, \quad \text{(XV)}$$

$$\text{Pt, } O_2, \text{ SrO}|SrF_2|\beta\text{-phase} + \alpha\text{-phase}, O_2, \text{ Pt}. \quad \text{(XVI)}$$

Since SrO, SrF_2, and O_2 gas must be in contact to fix the fluorine potential, SrF_2 powder was added to SrO in the preparation of the reference electrode pellet. Similarly, SrF_2 was also added to the measuring electrode pellet. Pellets were prepared by mixing component oxides and SrF_2 in 1 : 1 : 0.5 molar ratio, compacting at ~20 MPa and sintering in prepurified O_2 gas. The emf of each cell was first measured as a function of temperature under pure oxygen. Then, the emf was measured as a function of oxygen partial pressure in the gas phase at selected temperatures. The partial pressure was controlled using $Ar + O_2$ mixtures. In all cases, the same partial pressure of oxygen was maintained at both electrodes.

Each cell exhibited reproducible emfs only in a limited temperature range. The time required to obtain steady emf varied from ~20 h at 880 K to ~2 h at 1200 K. Reversibility of the cells was checked using microcoulometry, temperature cycling, and varying the gas flow rate over the electrodes.

III. RESULTS AND DISCUSSION

A. Phase relations

An isothermal section of the phase diagram of the system Bi–Sr–O at 1050 K composed from the results of this study is shown in Fig. 4. The bulk compositions of the samples analyzed are shown by cross marks. Twenty-five compositions were analyzed. The hatched composition ranges represent solution phases. All the oxygen-saturated liquid alloys and intermetallic compounds along the binary Bi–Sr were found to be in equilibrium with pure SrO. The oxygen solubility in the alloys was negligible. The oxygen chemical potential is expected to increase with concentration of Bi in the alloy in the two-phase fields involving the alloy and SrO. In three-phase fields, the oxygen potential has to be constant at a fixed temperature according to the phase rule. The compositions of all the compounds and solid solutions were confirmed by EDAX. The information obtained from XRD was consistent with crystallographic data in Table I. The ternary oxides $Bi_2Sr_3O_6$, $Bi_2Sr_2O_5$, Bi_2SrO_4, and solid solutions δ, β, and γ were in equilibrium with pure Bi metal. The Bi ion was found to be in the trivalent state in these interoxide compounds and solid solutions. It is therefore possible to equilibrate the coexisting phases along the pseudobinary Bi_2O_3–SrO with metallic Bi to fix the oxygen chemical potential which can be measured accurately using an oxide electrolyte. The interoxide compounds $Bi_2Sr_6O_{11}$, $Bi_{14}Sr_{24}O_{52}$, and $Bi_4Sr_6O_{15}$ were in equilibrium with pure O_2 gas. These oxides were not in equilibrium with alloys or intermetallics. The classical iodometric

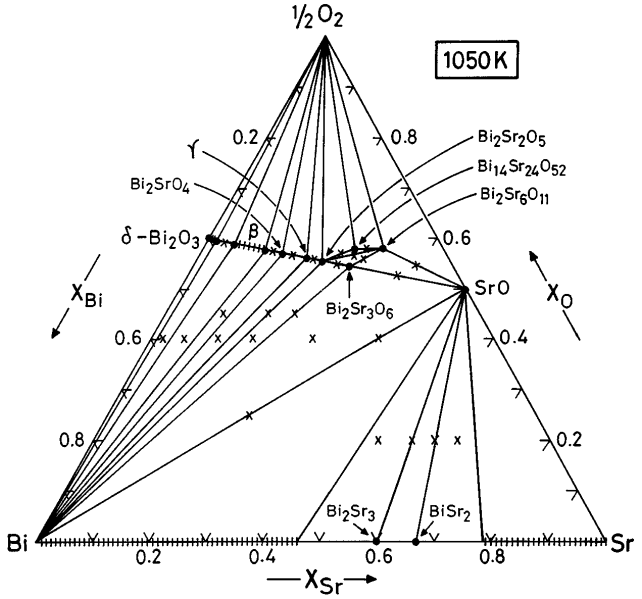

FIG. 4. Isothermal section of the phase diagram for the system Bi–Sr–O at 1050 K composed from the results of this study. The average composition of sample examined is shown by X.

method indicated that all the Bi ions in $Bi_2Sr_6O_{11}$, 50% of the Bi ions in $Bi_{14}Sr_{24}O_{52}$, and 75% of the Bi ions in $Bi_4Sr_6O_{15}$ were pentavalent. The ordering of pentavalent Bi ions in these structures requires further study. The compound $Bi_2Sr_6O_{11}$ was found to coexist with $Bi_2Sr_2O_5$ at reduced partial pressure in sealed capsule experiments: $Bi_{14}Sr_{24}O_{52}$ does not coexist with $Bi_2Sr_3O_6$ at 1050 K. Additional information on phase relations and stoichiometry of oxides obtained from emf measurements are discussed in Sec. III. C.

B. Chemical potential of Bi_2O_3

The reversible emfs of cells I to IV are plotted as a function of temperature in Fig. 5. The emfs of cells I to IV exhibit a change of slope at 1003(±1) K. This is related to the $\alpha \rightarrow \delta$ transformation of Bi_2O_3 in the reference electrode. The average value of the enthalpy of transformation deduced from the change in slope of emf is 30.6(±0.5) kJ/mol at 1003 K. The emf of cell IV exhibits a second change of slope at 904 K, related to the phase transition of the β-phase. The enthalpy of transition for the composition $Bi_{1.16}Sr_{0.42}O_{2.16}$ is 8.9(±2) kJ/mol. Within experimental uncertainty limits, the emfs of cells I to IV can be expressed as linear functions of temperature over most of the range, with changes in slope as identified in the figure. The change in slope is due to phase transition of one of the constituents of the electrodes. Expressions for the emf obtained by a least-squares regression analysis are summarized in Table II. Uncertainty estimates correspond to twice the standard deviation. The emf of cell IV for $T > 1050$ K is nonlinear, suggesting that the composition of the β-phase in equilibrium with Bi_2SrO_4 changes rapidly with temperature. The activity or chemical potential of Bi_2O_3 in various two-phase fields in the pseudobinary system Bi_2O_3–SrO can be deduced from the emfs of cells I to IV. The emf is directly related to the chemical potential of Bi_2O_3 by the relation,

$$-6FE = \Delta\mu_{Bi_2O3} = RT \ln a_{Bi_2O_3}. \quad (4)$$

The derived chemical potentials relative to α–Bi_2O_3 as the reference state are given in Table III.

C. Chemical potential of SrO

The variation of emfs of cells V to XV, operated under pure O_2, with temperature is displayed in Fig. 6. Reproducible emfs were obtained only in a limited temperature range for each cell. This may be related to the instability of one or more phases present at the electrodes. Some evidence for decomposition was obtained from XRD analysis of electrode pellets after emf measurements. The emfs of the cells, except for cells XI and XIV, vary linearly with temperature. The

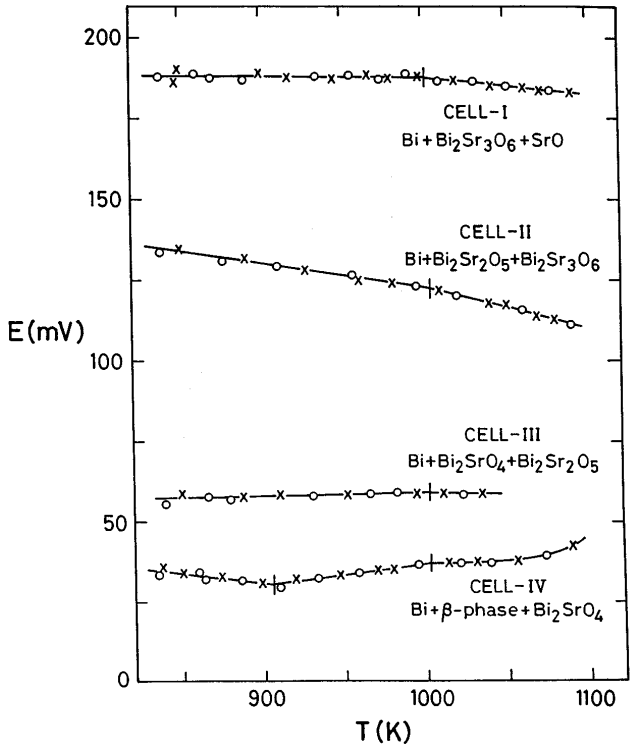

FIG. 5. Emf of cells I to IV based on $(Y_2O_3)ZrO_2$ as a function of temperature.

TABLE II. Emf of cells based on $(Y_2O_3)ZrO_2$.

Cell	E (mV)	Temperature (K)
I	$189.5 - 1.49 \times 10^{-3}\ T$ (±1.0)	840–1002
	$242.2 - 5.43 \times 10^{-2}\ T$ (±0.5)	1002–1090
II	$197.0 - 7.40 \times 10^{-2}\ T$ (±0.9)	840–1004
	$249.9 - 1.27 \times 10^{-1}\ T$ (±0.4)	1004–1090
III	$39.5 - 2.10 \times 10^{-2}\ T$ (±0.9)	840–1002
	$92.3 - 3.17 \times 10^{-2}\ T$ (±0.3)	1002–1038
IV	$79.8 - 5.39 \times 10^{-2}\ T$ (±0.8)	840– 906
	$-27.0 + 6.40 \times 10^{-2}\ T$ (±0.5)	906–1002
	Nonlinear: 37 (1020 K), 37 (1040 K), 38.3 (1060 K), 40.5 (1080 K), 42.5 (1090 K)	1002–1090

TABLE III. Chemical potential of Bi_2O_3 in two-phase fields of the pseudobinary system Bi_2O_3–SrO relative to α–Bi_2O_3.

Phase field	$\Delta\mu_{Bi_2O_3}$, J/mol
SrO + $Bi_2Sr_3O_6$	$-109{,}715 + 0.86\ T$ (±580)
$Bi_2Sr_3O_6$ + $Bi_2Sr_2O_5$	$-114{,}060 + 42.84\ T$ (±520)
$Bi_2Sr_2O_5$ + Bi_2SrO_4	$-22{,}870 - 12.16\ T$ (±520)
Bi_2SrO_4 + β_2	$-46{,}190 + 31.18\ T$ (±470)
Bi_2SrO_4 + β_1	$15{,}620 - 37.04\ T$ (±300) {840–1002 K}

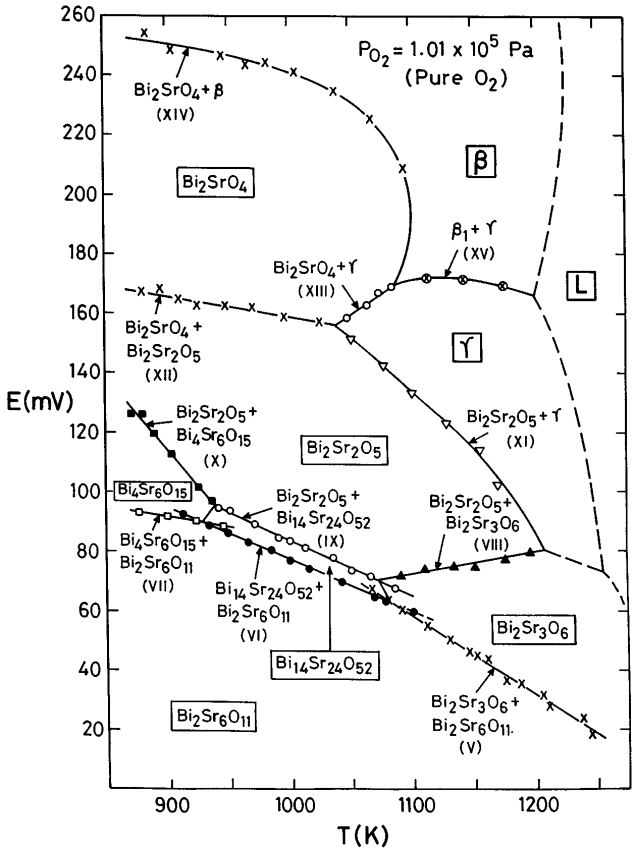

FIG. 6. Emf of cells V to XIV based on SrF_2 operated under pure O_2 as a function of temperature.

nonlinear variation of the emf of cell XI is probably related to the change in composition of the γ-phase with temperature. The highly nonlinear variation of the emf of cell XIV above 1000 K suggests significant change in the composition of β_1-phase with temperature. The results for cell XIV suggest congruent transformation of Bi_2SrO_4 to β_1 at 1100($\pm$5) K. Emfs of cells V and VI cross over at 1083($\pm$3) K, indicating decomposition of $Bi_{14}Sr_{24}O_{52}$ to $Bi_2Sr_3O_6$ and $Bi_2Sr_6O_{11}$ at higher temperatures in pure O_2. Similarly, emfs of cells VI and VII cross over at 928($\pm$3) K, signaling the decomposition of $Bi_{14}Sr_{24}O_{52}$ to $Bi_4Sr_6O_{15}$ and $Bi_2Sr_6O_{11}$ in pure oxygen. It is interesting to note that the stable emfs of cells V, VI, and VII are obtained $\sim$20 K above and below the stability domain of the phases involved. This suggest that metastable equilibrium exists at the electrodes, aided by the slow rate of decomposition of unstable phases. The lower temperature limit for the stability of $Bi_2Sr_3O_6$ is indicated by the intersection of the emfs of cells VIII and IX. Below 1073($\pm$3) K, $Bi_2Sr_3O_6$ decomposes to $Bi_{14}Sr_{24}O_{52}$ and $Bi_2Sr_2O_5$ in pure O_2. The compound $Bi_4Sr_6O_{15}$ decomposes to $Bi_2Sr_2O_5$ and $Bi_{14}Sr_{24}O_{52}$ above 938($\pm$3) K in O_2, as suggested by the interaction of the emfs of cells IX and X. The stability fields of $Bi_2Sr_6O_{11}$, $Bi_2Sr_3O_6$, $Bi_{14}Sr_{24}O_{52}$, and $Bi_4Sr_6O_{15}$ are clearly delineated by the emfs of cells V to X in Fig. 6. Phase relations in the ternary system Bi–Sr–O in pure oxygen can be deduced from the emf measurements using cells based on SrF_2 as the solid electrolyte. A projection of phase relations in the ternary Bi_2O_3–SrO–O (P_{O_2} = 1.01 $\times$ 10^5 Pa) from the oxygen apex on the Bi_2O_3–SrO isopleath is shown in Fig. 7 for $X_{SrO} > 0.45$. All the phases in the ternary Bi_2O_3–SrO–O in pure oxygen will be seen on the projection. The decomposition temperature of SrO_2 is calculated from thermodynamic data.[32] Clearly, phase relations in pure oxygen are substantially different from that in air (Fig. 1). The compound $Bi_{14}Sr_{24}O_{52}$ has a small stability range in pure oxygen, but is unstable in air. The change in slope of the emf-temperature plot for Bi_2SrO_4 + $Bi_2Sr_2O_5$ and Bi_2SrO_4 + β phase fields (cells XII and XIV, respectively) at 1098 K is related to phase transition of Bi_2SrO_4. The enthalpy of phase transition calculated from emf data is 4.83($\pm$1) kJ/mol.

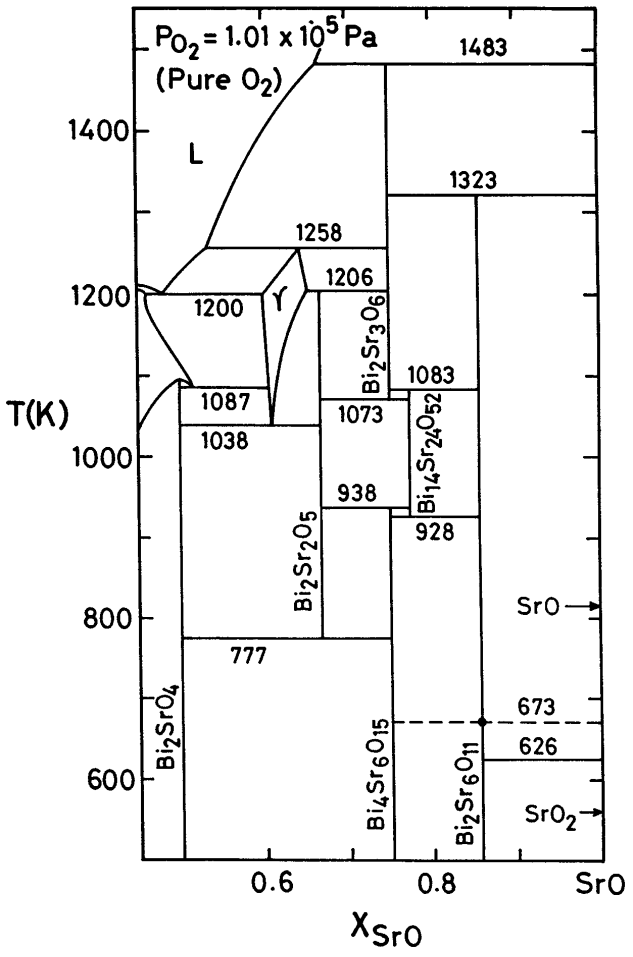

FIG. 7. Projection of phase relations in the system Bi_2O_3–SrO–O in pure oxygen at ambient pressure onto the Bi_2O_3–SrO isopleath.

D. Oxygen content of ternary oxides

If the ternary oxides present at the electrodes exhibit oxygen nonstoichiometry or contain excess oxygen to compensate for the presence of higher valent cations, emfs of cells with fluoride electrolytes will vary with the partial pressure of oxygen over the electrodes.[30,31] The emfs of cells V, VI, VII, IX, and X were found to be dependent on oxygen partial pressure in the gas phase over the electrodes. The emfs of the other cells incorporating SrF_2 were independent of oxygen partial pressure. Figure 8 shows the variation of emf of cell V with the logarithm of partial pressure at 1150 K. Emf can be represented by the expression,

$$E = 45.02 + 38.15 \log (P_{O_2}/P^\circ), \qquad (5)$$

where P° is the standard atmospheric pressure. The emf is zero when $\log(P_{O_2}/P^\circ) = -1.18$, indicating that SrO is present as a separate phase at unit activity below this value of partial pressure.

The activity of SrO at the working electrode of cell V is defined by the equation:

$$Bi_2Sr_6O_{11} \longrightarrow Bi_2Sr_3O_6 + 3SrO + O_2. \qquad (6)$$

When $Bi_2Sr_6O_{11}$ and $Bi_2Sr_3O_6$ are present at unit activity, the activity of SrO at the electrode and hence the emf are functions of the oxygen partial pressure. The slope of the line in Fig. 8 is a measure of the number of moles of gaseous oxygen involved in the electrode reaction, which in turn depends on the oxygen content of the ternary oxides. If the oxygen content of $Bi_2Sr_6O_{11}$ is considered to be unknown, the compound may be represented as $Bi_2Sr_6O_{9+x}$. Then $\partial E/\partial (\log P_{O_2})$ would be given by $(2.303x\ RT/12F)$. The value of x can be determined from the slope of the line in Fig. 8 as 2.007. Thus, the measurement of the emf of cell V as a function of the oxygen partial pressure confirms the stoichiometry suggested in the literature and the valency of the Bi ion determined by iodometry. Further, the value of partial pressure below which SrO precipitates as a separate phase can be used to derive the standard free energy change for reaction (6) at 1150 K, and cross-check the free energy data obtained independently.

The variation of the emfs of cells VI and IX with oxygen partial pressure at 1000 K is displayed in Fig. 9. The emfs of two cells converge at $\log(P_{O_2}/P^\circ) = -0.42$, suggesting decomposition of $Bi_{14}Sr_{24}O_{52}$ to $Bi_2Sr_2O_5$ and $Bi_2Sr_6O_{11}$ below this partial pressure:

$$Bi_{14}Sr_{24}O_{52} \longrightarrow 4.5Bi_2Sr_2O_5 + 2.5Bi_2Sr_6O_{11} + O_2. \qquad (7)$$

The experimental determination of the partial pressure provides an additional check on the Gibbs energies of formation of the three ternary oxides involved. The activity of SrO at the working electrodes of cells VI and IX are defined by the equations:

$$Bi_{14}Sr_{24}O_{52} + 18SrO + 3.5O_2 \longrightarrow 7Bi_2Sr_6O_{11}, \qquad (8)$$

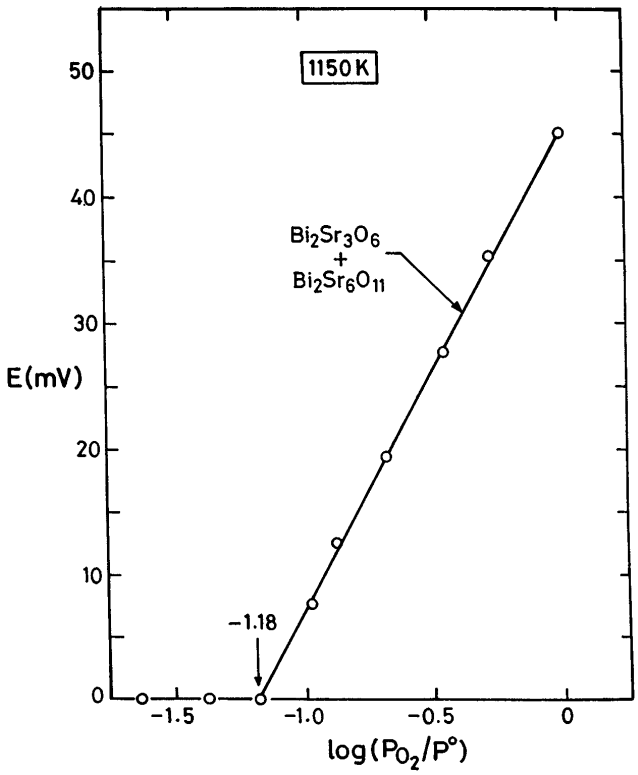

FIG. 8. Variation of the emf of the cell V with partial pressure of oxygen over the electrodes at 1150 K. $P^\circ = 1.01 \times 10^5$ Pa.

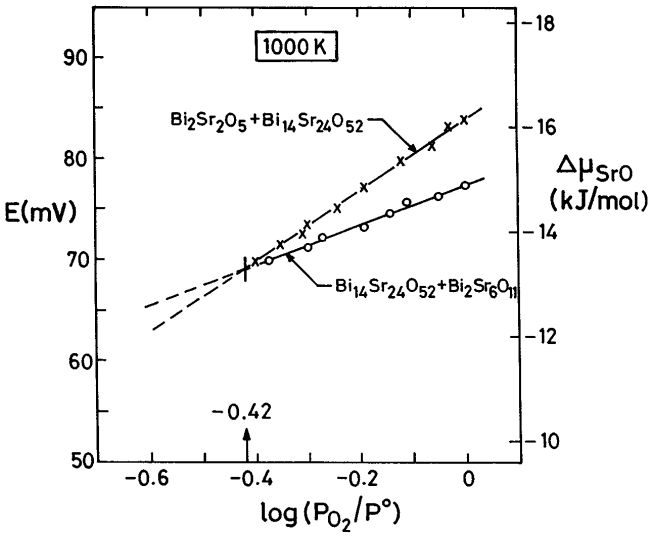

FIG. 9. Variation of emfs of cells VI and IX with partial pressure of oxygen over the electrodes at 1000 K. $P^\circ = 1.01 \times 10^5$ Pa.

$$Bi_{14}Sr_{24}O_{52} \longrightarrow 7Bi_2Sr_2O_5 + 10SrO + 3.5O_2\,, \qquad (9)$$

respectively. When the two ternary oxides involved in each reaction are present at unit activity, the activity of SrO and hence the emf are functions of oxygen partial pressure. The values of $\partial E/\partial(\log P_{O_2})$ obtained by experiment are almost identical to values calculated from Eqs. (8) and (9). The oxygen content of $Bi_{14}Sr_{24}O_{52}$ is thus confirmed. Similar studies on the variation of emfs of cells VII and X with oxygen partial pressure confirm the oxygen stoichiometry of $Bi_4Sr_6O_{15}$.

Expressions for the emf of cells V and XV obtained by least-squares regression analysis are given in Table IV. When oxygen at the same partial pressure is present over both the electrodes, the relative chemical potential of SrO at the working electrode can be directly obtained from the emf of cells incorporating SrF_2 as the solid electrolyte:

$$\Delta\mu_{SrO} = -2FE\,. \qquad (10)$$

Equations for the chemical potential of SrO deduced from emfs are presented in Table V.

E. Gibbs energies of formation of the interoxide compounds and solid solutions

The standard Gibbs energies of formation of ternary oxides and solid solutions can be derived from the emf of the various cells. The overall plan of deployment of the emf data for deriving and cross-checking thermodynamic properties of various phases is shown in Fig. 10. The scheme is not unique. Thermodynamic properties of ternary phases can be calculated with slightly reduced accuracy using other combinations of emfs. The standard Gibbs energy of formation of each ternary oxide on the pseudobinary Bi_2O_3–SrO join can be computed from the chemical potentials of Bi_2O_3 and SrO in phase fields involving the compound. Thus, two values for the free energy of formation can be derived from chemical potentials of component binary oxides on either side of a ternary compound using Eq. (2). The two values for the Gibbs energy thus derived for each compound are

TABLE IV. Emf of cells based on SrF_2.

Cell	E (mV)	Temperature (K)
V	$344.5 - 2.60 \times 10^{-1}\,T$ ($\pm$1.0)	1065–1245
VI	$251.1 - 1.74 \times 10^{-1}\,T$ ($\pm$0.5)	910–1100
VII	$156.3 - 7.20 \times 10^{-2}\,T$ ($\pm$0.5)	875– 950
VIII	$-7.5 + 7.25 \times 10^{-2}\,T$ ($\pm$0.6)	1090–1200
IX	$266.2 - 1.83 \times 10^{-1}\,T$ ($\pm$0.6)	940–1090
X	$556.8 - 4.93 \times 10^{-1}\,T$ ($\pm$1)	870– 940
XI	Nonlinear: 142 (1077 K), 133 (1101 K), 123 (1128 K), 114 (1155 K), 102 (1169 K)	1070–1170
XII	$228.7 - 7.00 \times 10^{-2}\,T$ ($\pm$1)	880–1030
XIII	$-137.0 + 2.82 \times 10^{-1}\,T$ ($\pm$0.5)	1040–1087
XIV	$334.7 - 9.33 \times 10^{-2}\,T$ ($\pm$1)	880–1005
	Nonlinear: 234 (1038 K), 224.5 (1068 K), 208 (1095 K)	$T > 1005$
XV	Nonlinear: 172 (1114 K), 171 (1143 K), 170 (1175 K)	1087–1200
XVI	$215.2 + 2.14 \times 10^{-1}\,T$ ($\pm$2)	880– 990

TABLE V. Chemical potential of SrO in two-phase fields of the system Bi–Sr–O in pure oxygen.

Phase field	$\Delta\mu_{Bi_2O_3}$, J/mol
$Bi_2Sr_6O_{11} + Bi_2Sr_3O_6$	$-66{,}485 + 50.18\,T$ ($\pm$200)
$Bi_2Sr_6O_{11} + Bi_{14}Sr_{24}O_{52}$	$-48{,}460 + 33.58\,T$ ($\pm$100)
$Bi_2Sr_6O_{11} + Bi_4Sr_6O_{15}$	$-30{,}165 + 13.90\,T$ ($\pm$100)
$Bi_2Sr_3O_6 + Bi_2Sr_2O_5$	$1450 - 13.99\,T$ ($\pm$120)
$Bi_{14}Sr_{24}O_{52} + Bi_2Sr_2O_5$	$-51{,}375 + 35.32\,T$ ($\pm$120)
$Bi_4Sr_6O_{15} + Bi_2Sr_2O_5$	$-107{,}460 + 95.14\,T$ ($\pm$200)
$Bi_2Sr_2O_5 + \gamma$-phase	$-27{,}405$ (1077 K), $-25{,}670$ (1101 K), $-23{,}740$ (1128 K), $-22{,}000$ (1155 K), $-19{,}685$ (1169 K)
$Bi_2Sr_2O_5 + Bi_2SrO_4$	$-44{,}140 + 13.51\,T$ ($\pm$200)
γ-phase + Bi_2SrO_4	$26{,}400 - 54.42\,T$ ($\pm$100) {1040–1087 K}
$Bi_2SrO_4 + \beta$-phase	$-64{,}595 + 18.01\,T$ ($\pm$200) {880–1005 K}, $-45{,}160$ (1038 K), $-43{,}330$ (1068 K), $-40{,}140$ (1095 K)
β-phase + γ-phase	$-33{,}195$ (1114 K), $-33{,}000$ (1143 K), $-32{,}810$ (1075 K)
β-phase + α-phase	$-41{,}530 - 41.30\,T$ ($\pm$400) {880–990 K}

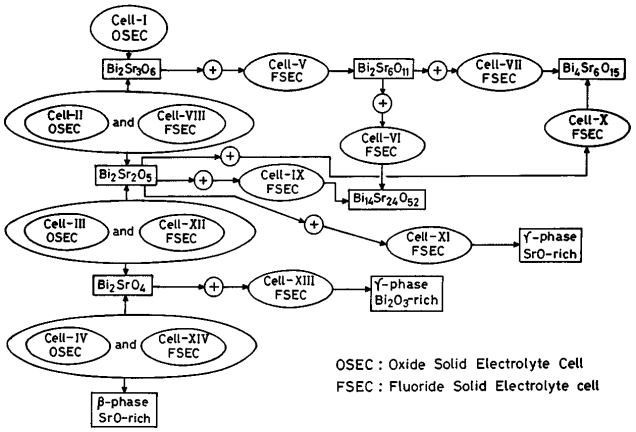

FIG. 10. Plan for the deployment of emf data on various cells for deriving and cross-checking Gibbs energies of formation of ternary oxides and solid solutions. The ⊕ sign indicates that Gibbs energy of formation of the preceding phase is combined with measurements on the designated cell to obtain the properties of the following phase on the diagram.

found to be in close agreement, indicating good internal consistency. The maximum difference in the value of $\Delta G_f^0(Bi_{2m}Sr_nO_{3m+n})/(m + n)$ is 350 J/mol of component binary oxides. The mean values for the integral free energy of formation of the interoxide compounds and solid solutions are given in Table VI, except for Bi_2SrO_4. For this compound, the value obtained from the emf of cells III and XII appear to be more consistent with the properties of the γ-phase and phase diagram than those derived from the emfs of cells IV and XIV. For the solid solution phases β and γ, only one value is obtained from emf at fixed composition and temperature.

Gibbs energies of compounds containing Bi^{5+} ions ($Bi_2Sr_6O_{11}$, $Bi_4Sr_6O_{15}$, and $Bi_{14}Sr_{24}O_{52}$) are derived relative to those for $Bi_2Sr_3O_6$ and $Bi_2Sr_2O_5$ using emf of cells based on SrF_2, as indicated in Fig. 10. The difference between the two sets of values calculated for $Bi_4Sr_6O_{15}$, according to the scheme in Fig. 10, is $\sim$700 J/mol; for $Bi_{14}Sr_{24}O_{52}$ the difference is $\sim$2000 J/mol. The average values are given in Table VI.

Gibbs energies of formation of ternary phases in the system Bi–Sr–O have not been reported in the literature. However, the chemical potential of SrO for some compositions has been measured by Baek and Virkar.[27] Their values are compared with results obtained in this work in Fig. 11. The agreement is satisfactory. Information on standard Gibbs free energies of formation of ternary oxides and solid solutions, obtained for the first time in this study, permit computation of phase diagrams at different oxygen partial pressures. Chemical potential diagrams can also be composed from the present results at different temperatures.

Idemoto *et al.*[28] measured enthalpies of formation of five ternary phases at 298 K by solution calorimetry using 1.53 M $HClO_4$. The "second-law" enthalpies of formation of ternary oxides from binary oxides (Bi_2O_3 + SrO) and O_2 (where required) obtained in this study at a mean temperature of 1000 K are compared with calorimetric information in Table VII. There is good agreement, except for the β-phase and $Bi_2Sr_6O_{11}$. Information on the β-phase obtained in the two studies are for different compositions. The enthalpy of formation of the β-phase is expected to be a strong function of composition, becoming more negative with SrO concentration. For the compound $Bi_2Sr_6O_{11}$, calorimetric data are more negative than the value obtained in this study by 233.3 kJ/mol. Bi^{5+} ions were probably present in solution when the compound was dissolved in acid during calorimetric measurement. Hence, by subtracting the enthalpies of solution of Bi_2O_3 and SrO in acid from the enthalpy of solution of the compound, the correct value of enthalpy of formation of the compound would not be obtained. An unknown enthalpy of oxidation of Bi^{3+} to Bi^{5+} in solution is required to derive the correct value for the enthalpy of formation of $Bi_2Sr_6O_{11}$. Incorrect determination of the valency of Bi in the ternary oxide by Idemoto *et al.*[28] led to a faulty calorimetric strategy.

IV. SUMMARY

An isothermal section of the phase diagram for the system Bi–Sr–O at 1050 K was established. Several compositions in the ternary were quenched after equilibration, and phases present were identified by optical microscopy, XRD, and EDAX. Five ternary oxides (Bi_2SrO_4, $Bi_2Sr_2O_5$, $Bi_2Sr_3O_6$, $Bi_{14}Sr_{24}O_{52}$, and $Bi_2Sr_6O_{11}$) and three solid solution phases (δ, β, and γ) were identified at 1050 K. Another ternary compound $Bi_4Sr_6O_{15}$ was found to be stable at lower temperatures. The presence of pentavalent bismuth was confirmed in compounds $Bi_4Sr_6O_{15}$, $Bi_{14}Sr_{24}O_{52}$, and $Bi_2Sr_6O_{11}$ by iodometry.

Based on the phase diagram, sixteen galvanic cells were designed to measure the activity of Bi_2O_3 and SrO in various phase fields. A yttria-stabilized zirconia solid electrolyte was used to measure the oxygen potential of oxide mixtures in equilibrium with metallic bismuth. A single-crytal SrF_2 solid electrolyte was used to measure the activity of SrO in oxide mixtures under controlled oxygen partial pressures. The emf data allowed independent assessments of the stability of ternary oxides. Data from the different cells were found to be internally consistent. The free energies of formation of ternary phases from the component binary oxides (and oxygen

TABLE VI. Integral molar free energies of formation of interoxide compounds and solid solutions.

Formation reaction	ΔG_f^0, J/mole	Temperature (K)
α–Bi_2O_3 + 3SrO → $Bi_2Sr_3O_6$	−109,700 + 0.86 T (±650)	840–1090
α–Bi_2O_3 + 2SrO → $Bi_2Sr_2O_5$	−111,155 + 14.85 T (±650)	840–1200
α–Bi_2O_3 + SrO → Bi_2SrO_4	−67,010 + 1.35 T (±550)	840–1098
α–Bi_2O_3 + 6SrO + O_2 → $Bi_2Sr_6O_{11}$	−309,130 + 151.41 T (±900)	1073–1250
2α–Bi_2O_3 + 6SrO + 1.5O_2 → $Bi_4Sr_6O_{15}$	−437,250 + 219.8 T (±1900)	870– 938
7α–Bi_2O_3 + 24SrO + 3.5O_2 → $Bi_{14}Sr_{24}O_{52}$	−1,291,730 + 456.3 T (±6600)	928–1083
0.39α–Bi_2O_3 + 0.61SrO → $Bi_{0.78}Sr_{0.61}O_{1.78}$ (γ)	−20,330 − 11.45 T (±200)	1038–1175
0.58α–Bi_2O_3 + 0.42SrO → $Bi_{1.16}Sr_{0.42}O_{2.16}$ (β_2)	−26,970 − 4.14 T (±400)	840– 906
0.58α–Bi_2O_3 + 0.42SrO → $Bi_{1.16}Sr_{0.42}O_{2.16}$ (β_1)	−18,070 − 13.92 T (±200)	906–1090

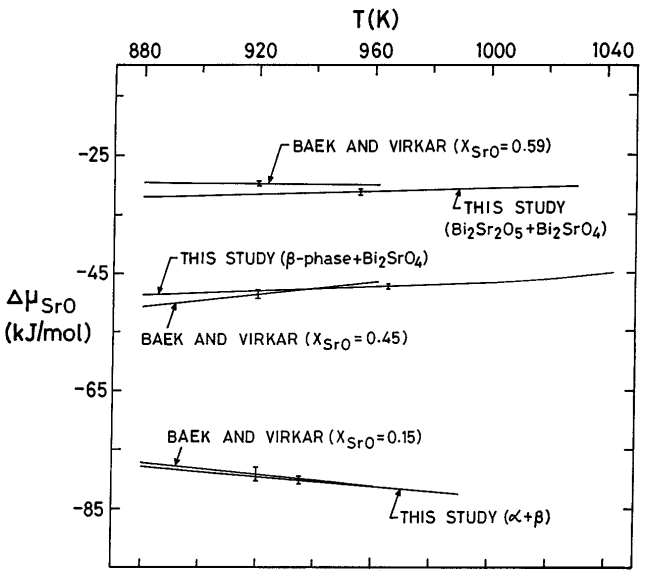

FIG. 11. Comparison of the chemical potential of SrO obtained in this study with the measurements of Baek and Virkar.[27]

TABLE VII. Comparison of enthalpies of formation of ternary oxides from component binaries (and oxygen) obtained from emf data and calorimetry.[28]

	ΔH_f^0 (kJ/mol)	
Compound	This study, emf	Idemoto *et al.*,[28] calorimetry
Bi_2SrO_4	−67.0 (±3)	−62.9 (±10.8)
$Bi_2SrO_2O_5$	−111.2 (±4)	−115.2 (±6)
$Bi_2Sr_3O_6$	−109.7 (±5)	−105.0 (±12)
$Bi_2Sr_6O_{11}$	−309.1 (±8)	−542.4 (±22.4)
γ	−20.3 (+1)	−21.9 (±2.7)
	$X_{SrO} = 0.61$	$X_{SrO} = 0.62$
β_2	−26.97 (±3)	−19.04 (±3)
	($Bi_{1.16}Sr_{0.42}O_{2.16}$)	($Bi_{1.34}Sr_{0.33}O_{2.34}$)

gas) in the temperature range 850 to 1100 K are given by the following equations:

$$Bi_2SrO_4: \quad \Delta G_f^0(0x) = -67,020 + 1.35T \ J/\text{mol},$$

$$Bi_2Sr_2O_5: \quad \Delta G_f^0(0x) = -111,150 + 14.85T \ J/\text{mol},$$

$$Bi_2Sr_3O_6: \quad \Delta G_f^0(0x) = -109,700 + 0.86T \ J/\text{mol},$$

$$Bi_4Sr_6O_{15}: \quad \Delta G_f^0(0x + O_2) = -437,250 + 219.8T \ J/\text{mol},$$

$$Bi_{14}Sr_{24}O_{52}: \quad \Delta G_f^0(0x + O_2) = -1,291,730 + 456.3T \ J/\text{mol},$$

$$Bi_2Sr_6O_{11}: \quad \Delta G_f^0(0x + O_2) = -309,130 + 151.6T \ J/\text{mol}.$$

The standard state for Bi_2O_3 is the low-temperature crystalline α form. The second law enthalpies of formation of ternary oxides are in good accord with calorimetric information, except for the β-phase and $Bi_2Sr_6O_{11}$. The source of the discrepancy for $Bi_2Sr_6O_{11}$ is identified. Using a novel variation of the galvanic cell technique, in which the emf of a cell incorporating a fluoride electrolyte and oxide electrodes is measured as a function of oxygen potential of the gas phase, oxygen contents of the ternary oxides were confirmed. Improved data obtained in this study can be used to compute phase equilibria in higher order systems as a function of temperature and oxygen partial pressure. Equilibrium phase diagrams are excellent guides for the development and optimization of new processing routes for high T_c oxide superconductors.

REFERENCES

1. R. Guillermo, P. Conflant, J. C. Boivin, and D. Thomas, Rev. Chim. Mineral. **15**, 153 (1978).
2. P. Conflant, M. Drache, J. P. Wignacourt, and J. C. Boivin, Mater. Res. Bull. **26**, 1219 (1991).
3. E. M. Levin and R. S. Roth, J. Res. Nat. Bur. Stand., Sec. A **68**, 197 (1964).
4. R. S. Roth, C. J. Rawn, B. P. Burton, and F. Beech, J. Res. Natl. Inst. Stand. Technol. **95**, 291 (1990).
5. N. M. Hwang, R. S. Roth, and C. J. Rawn, J. Am. Ceram. Soc. **73**, 2531 (1990).
6. E. Yu. Vstavskaya, A. Yu. Zuev, V. A. Chereponov, S. D. Sutton, and J. S. Abell, J. Phase Equil. **15**, 573 (1994).
7. F. Abbattista, C. Brisi, D. Mazza, and M. Vallino, Mater. Res. Bull. **26**, 107 (1991).
8. K. T. Jacob and T. Mathews, J. Mater. Chem. **1**, 545 (1991).
9. B. V. Slobodin, I. A. Ostapenko, and A. A. Fotiev, Inorg. Mater. **27**, 2220 (1992).
10. K. T. Jacob and K. P. Jayadevan, Mater. Trans. JIM **38**, 427 (1997).
11. T. Takahashi, H. I. Iwahara, and Y. Nagai, J. Appl. Electrochem. **2**, 97 (1972).
12. M. V. Zinkevich, S. A. Prodan, Yu. G. Zonor, and V. V. Vashuk, Inorg. Mater. **31**, 129 (1995).
13. T. Mathews, Ph.D. Thesis, Department of Metallurgy, Indian Institute of Science, Bangalore, India (1993).
14. H. A. Harwig, Z. Anorg. Allg. Chem. **444**, 151 (1978).
15. D. Taylor, Trans. J. British Ceram. Soc. **83**, 5 (1978).
16. K. J. Range, F. Rau, U. Schiessl, and U. Klement, Z. Anorg. Allg. Chem. **620**, 879 (1994).
17. B. Eisenmann and K. Deller, Z. Naturforsch **30B**, 66 (1975).
18. D. Mercurio, J. C. C. Mesjard, B. Frit, P. Conflant, J. C. Boivin, and T. Vogt, J. Solid State Chem. **112**, 1 (1994).
19. R. L. Withers and H. Rossel, J. Solid State Chem. **118**, 66 (1995).
20. T. A. M. Haemers and D. J. W. Ijdo, Mater. Res. Bull. **26**, 989 (1991).
21. C. C. Torardi, J. B. Parise, A. Santoro, C. J. Rawn, R. S. Roth, and B. P. Burton, J. Solid State Chem. **93**, 228 (1991).
22. P. Conflant and J. C. Boivin, C. R. Acad. Sci., Ser. C., Sci. Chim. **288**, 161 (1979).
23. J. F. Vente, R. B. Helmholdt, and D. J. W. Ijdo, Acta Crystallogr. **C48**, 1380 (1992).
24. Bokhimi and M. Portilla, J. Solid State Chem. **105**, 371 (1993).

25. P. Conflant, M. Drache, M. Lagrenee, J. C. Boivin, and J. P. Wignacourt, Solid State Ionics **53–56**, 592 (1992).
26. Y. Ikeda, H. Ito, S. Shimomura, Y. One, K. Inaba, Z. Hiroi, and M. Takano, Physica C **159**, 93 (1989).
27. H. D. Baek and A. V. Virkar, J. Electrochem. Soc. **139**, 3174 (1992).
28. Y. Idemoto, K. Shizuka, Y. Yasuda, and K. Fueki, Physica C **211**, 36 (1993).
29. R. Horyn, M. Wolcyrz, and R. Andruszkiewicz, J. Alloys Compounds **191**, 203 (1993).
30. K. T. Jacob and T. Mathews, J. Am. Ceram. Soc. **75**, 3225 (1992).
31. T. Mathews, J. P. Hajra, and K. T. Jacob, Chem. Mater. **5**, 1669 (1993).
32. M. W. Chase, Jr., C. A. Davies, J. R. Downey, Jr., D. J. Fruip, R. A. McDonald, and A. N. Syverud, *Janaf Thermochemical Tables,* 3rd ed. J. Phys. Chem. Ref. Data **14**, Supplements 1 and 2 (1985).